

One-loop weak corrections to Higgs production

Valentin Hirschi¹, Simone Lionetti², and Armin Schweitzer³

^{1,3}*ETH Zürich, Rämistrasse 101, 8092 Zürich, Switzerland*

²*Institute for Particle Physics Phenomenology, Durham University, Durham DH1 3LE, UK*

Abstract

We compute mixed QCD-weak corrections to inclusive Higgs production at the LHC from the partonic process $gg \rightarrow Hq\bar{q}$. We start from the UV- and IR-finite one-loop weak amplitude and consider its interference with the corresponding one-loop QCD amplitude. This contribution is a $\mathcal{O}(\alpha_s\alpha)$ correction to the leading-order gluon-fusion cross section, and was not numerically assessed in previous works. We also compute the cross section from the square of this weak amplitude, suppressed by $\mathcal{O}(\alpha^2)$. Finally, we consider contributions from the partonic process $gq \rightarrow Hq$, which are one order lower in α_s , as a reference for the size of terms which are not enhanced by the large gluon luminosity. We find that, given the magnitude of the uncertainties on current state-of-the-art predictions for Higgs production, all contributions computed in this work can be safely ignored, both fully inclusively and in the boosted Higgs regime. This result supports the approximate factorisation of QCD and weak corrections to that process.

Contents

1	Introduction	2
2	Classification of contributions	4
3	Initial-state collinear singularities	7
4	Setup of the computation and numerical results	9
5	Conclusion	12
Appendix A Initial-collinear counterterms		14
Appendix B Analytical computation of the amplitudes $A_{gg \rightarrow Hq\bar{q}}^{(2,0)}$ and $A_{gg \rightarrow Hq\bar{q}}^{(0,2)}$		18
Appendix C Validation material		23

1 Introduction

In the quest towards an ever more accurate prediction for the inclusive Higgs production cross section at hadron colliders, one of the major tasks is the computation of fixed-order corrections in the perturbative expansion in powers of the Standard Model (SM) couplings. Our understanding of pure QCD corrections, which are known to be very important for this process, has reached an unprecedented level of accuracy in recent times. A milestone in this programme was achieved with the computation of the third correction term in the expansion in the strong coupling α_s of the cross section for Higgs production via gluon fusion in the infinite top mass limit [1, 2]. In a typical setup for the LHC running at a centre-of-mass energy of 13 TeV, this contribution shifts the prediction for the total cross section upwards by roughly 3% [3].

On the other hand, weak corrections to the leading-order (LO) inclusive Higgs cross section also need to be considered. In the same setup mentioned before, the first weak term turns out to increase the total gluon fusion cross section by a significant 5% [4–6]. Since next-to-leading-order (NLO) QCD corrections can be as large as the leading contribution, the motivation to investigate mixed first-order QCD and first-order weak corrections is very strong. Although the exact size of this term is at present unknown, various approximations have been considered in the literature. The first estimate to appear was based on the argument that mixed QCD-weak effects on the inclusive Higgs production cross section are well approximated by combining the purely weak term and the full QCD series in a multiplicative fashion [7]. Following this *factorisation* approach, the authors of ref. [3] reported the mixed QCD-weak corrections to be approximately 3% of the full result, and conservatively estimated the uncertainty stemming from non-factorisable contributions to be 1% of the total.

The estimates of [3, 7] are obtained by considering the unphysical limit $m_H \ll m_W, m_Z$. The gluon induced interference contributions discussed in our work are suppressed in this limit by two powers of the weak boson masses with respect to the leading order $\mathcal{O}(\alpha_S^2 \alpha)$ cross section, which we verified by explicit calculation. The theoretical uncertainty associated to each of the other main error sources (determination of parton distribution functions, truncation of the QCD perturbative series, and missing quark-mass effects) is currently of the same order. It is therefore highly desirable to remove the ambiguity due to the factorisation approximation.

Important steps have recently been made in this direction. Thanks to the calculation of the three-loop mixed QCD-weak correction to Higgs boson gluon fusion for arbitrary masses of the W , Z , and Higgs bosons [8], an estimate of the cross section in the soft-virtual approximation was obtained [9]. An independent work considered three-loop matrix elements in the limit of massless vector bosons instead, and combined them with a different class of two-loop real-emission contributions [10]. The estimates obtained using these approximations support the validity of the factorisation approach, since they include some non-factorisable effects and find that these are numerically small.

In order for the full mixed QCD-weak term to become available, however, two pieces of the puzzle are still missing. On the one hand there is the formidable challenge of computing two-loop matrix elements with an extra real emission for arbitrary W , Z , and Higgs masses. On the other hand, there are UV- and IR-finite one-loop weak contributions to the production of the Higgs in association with two partons, which feature more complicated kinematics but whose one-loop integrals are well understood. Although in general corrections with fewer or soft real emissions are expected to dominate within the inclusive cross section [9], the contributions with two extra hard partons are formally of the same order and may disrupt the approximate factorisation of weak and QCD corrections because of their final-state kinematic structure.

In the present paper, we address this issue by carrying out the exact *inclusive* computation of the contribution to mixed QCD-weak corrections from the one-loop partonic subprocess $gg \rightarrow Hq\bar{q}$. We stress that this contribution features one-loop pentagon topologies which appear only in matrix elements with (at least) two real emissions, that do not fit in a factorised picture and that have not been assessed before.

The paper proceeds as follows. In Section 2, we discuss the different contributions that enter our computation, we categorise them and identify potential competing mechanisms which are formally of the same order or slightly higher. Although the computation of the required matrix elements is straightforward using standard public codes for one-loop calculations, the computation of the pieces of cross sections we are interested in requires the renormalisation of parton distributions and the subtraction of initial-state collinear singularities. Given the very special features of the process examined, these steps require some care and are thus described in Section 3. Finally, we report and discuss numerical results.

2 Classification of contributions

In order to classify contributions to the Higgs inclusive cross section, it is useful to write its mixed QCD and weak expansion as

$$\sigma_{pp \rightarrow H+X} = \sum_{m,n} \sigma_{pp \rightarrow H+X}^{(m,n)}, \quad \text{where} \quad \sigma_{pp \rightarrow H+X}^{(m,n)} \propto \alpha_s^{m+2} \alpha^{n+1}, \quad (2.1)$$

where the prefactor $\alpha_s^2 \alpha^1$ is chosen so as to match the couplings factorised by the leading-order loop-induced gluon-fusion contribution to inclusive Higgs production. Notice that we group all squared couplings that are not strong, including the Yukawa of the top quark, under the label α , in view of their comparable strength and of the electroweak gauge relations often rendering their separate factorisation ambiguous. The corrections often labelled “QCD N^mLO” and “(electro)weak NⁿLO” are then denoted by $\sigma_{pp \rightarrow H+X}^{(m,0)}$ and $\sigma_{pp \rightarrow H+X}^{(0,n)}$, as they become impractical when addressing the mixed cases $\sigma_{pp \rightarrow H+X}^{(m,n)}$. With such a notation in mind, the expected naive parametric suppression from the couplings, which counts $\alpha_s \sim 10^{-1}$ and $\alpha \sim 10^{-2}$, simply reads $\sigma_{pp \rightarrow H+X}^{(m,n)} \sim 10^{-m-2n}$. In order to discuss interference terms, we also find it useful to introduce a similar notation for amplitudes:

$$A_{ab \rightarrow H+X}^{(i,j)} \propto g_s^{i+2} g^{j+1}, \quad (2.2)$$

where we denote by g all couplings that are not g_s .

As mentioned above, weak and QCD corrections are expected to factorise to a certain degree, such that

$$\sigma_{pp \rightarrow H+X}^{(m,n)} \sim \sigma_{pp \rightarrow H+X}^{(m,0)} \cdot \sigma_{pp \rightarrow H+X}^{(0,n)}. \quad (2.3)$$

This approximation is valid under the assumption that the main contributions to the mixed QCD-weak cross section are to be attributed either to soft gluons or Sudakov weak logarithms. If one is to assess violations of this factorisation, the expansion term $\sigma_{pp \rightarrow H+X}^{(1,1)}$ must be computed *exactly*. We now set out to discuss the many contributions this term receives.

In this work, we only consider *weak* corrections involving the W and Z bosons, as these dominate over the genuine electroweak corrections (*i.e.* unresolved *photon* exchange or emission) to contributions where the Higgs is produced from massive quark loop lines that are not the top-quark.

Also, the gluon initiated processes are expected to be the dominant contributions at the LHC, where quark parton distribution functions (PDFs) are small in comparison to the gluon one for the typical values of the Bjorken x ’s probed by the kinematics involved. We therefore neglect all contributions to $\sigma_{pp \rightarrow H+X}^{(1,1)}$ that factorise parton luminosities with at least one quark. To get a reference for the size of these terms that we do not compute, we report numerical results also for $\sigma_{gq \rightarrow Hq}^{(0,1)}$.¹

¹Note that our initial-state notation gq encompasses in this context both permutations gq and qg .

Weak corrections stemming from the interference with leading QCD production modes are often subject to kinematic suppressions that renders them smaller than what is naively expected from their factorised couplings. For this reason, we also report the pieces of the cross sections $\sigma_{gg \rightarrow Hq\bar{q}}^{(0,2)}$ and $\sigma_{gq \rightarrow Hq}^{(-1,2)}$ built from the square of the amplitudes $A_{gg \rightarrow Hq\bar{q}}^{(0,2)}$ and $A_{gq \rightarrow Hq}^{(-1,2)}$. These form a gauge-invariant subset of higher-order contributions.

Our work reports on the contribution $\sigma_{gg \rightarrow Hq\bar{q}}^{(1,1)}$ for the first time and, together with the results from refs. [7, 9], it completes the computation of $\sigma_{gg \rightarrow H+X}^{(1,1)}$. We now proceed to list in Table 1 all amplitudes building $\sigma_{gp \rightarrow H+X}^{(1,1)}$.

\times	$A_{gg \rightarrow H}^{(0,0)\star}$	$A_{gg \rightarrow H}^{(2,0)\star}$	$A_{gg \rightarrow H}^{(0,2)\star}$	$A_{gg \rightarrow H}^{(2,2)\star}$	$A_{gg \rightarrow Hg}^{(1,0)\star}$	$A_{gg \rightarrow Hg}^{(1,2)\star}$	$A_{gg \rightarrow Hq\bar{q}}^{(2,0)\star}$	$A_{gg \rightarrow Hq\bar{q}}^{(0,2)\star}$
$A_{gg \rightarrow H}^{(0,2)}$	$\sigma_{gg \rightarrow H}^{(0,1)}$	$\sigma_{gg \rightarrow H}^{(1,1)}$	$\sigma_{gg \rightarrow H}^{(0,2)}$	$\sigma_{gg \rightarrow H}^{(1,2)}$				
$A_{gg \rightarrow H}^{(2,2)}$	$\sigma_{gg \rightarrow H}^{(1,1)}$	$\sigma_{gg \rightarrow H}^{(2,1)}$	$\sigma_{gg \rightarrow H}^{(1,2)}$	$\sigma_{gg \rightarrow H}^{(2,2)}$				
$A_{gg \rightarrow Hg}^{(1,2)}$					$\sigma_{gg \rightarrow Hg}^{(1,1)}$	$\sigma_{gg \rightarrow Hg}^{(1,2)}$		
$A_{gg \rightarrow Hq\bar{q}}^{(0,2)}$							$\sigma_{gg \rightarrow Hq\bar{q}}^{(1,1)}$	$\sigma_{gg \rightarrow Hq\bar{q}}^{(0,2)}$

\times	$A_{gq \rightarrow Hq}^{(1,0)\star}$	$A_{gq \rightarrow Hq}^{(3,0)\star}$	$A_{gq \rightarrow Hq}^{(-1,2)\star}$	$A_{gq \rightarrow Hq}^{(1,2)\star}$
$A_{gq \rightarrow Hq}^{(-1,2)}$	$\sigma_{gq \rightarrow Hq}^{(0,1)}$	$\sigma_{gq \rightarrow Hq}^{(1,1)}$	$\sigma_{gq \rightarrow Hq}^{(-1,2)}$	$\sigma_{gq \rightarrow Hq}^{(0,2)}$
$A_{gq \rightarrow Hq}^{(1,2)}$	$\sigma_{gq \rightarrow Hq}^{(1,1)}$	$\sigma_{gq \rightarrow Hq}^{(2,1)}$		$\sigma_{gq \rightarrow Hq}^{(1,2)}$

Table 1: Summary of contributing amplitudes to the weak corrections to Higgs inclusive production involving one (bottom table) and two (top table) initial-state gluons, for various perturbative orders. The results reported in this work are highlighted with a green background, while those addressed in ref. [7, 9] are denoted in blue. Together, these form the *complete* $\sigma_{gg \rightarrow H+X}^{(1,1)}$ weak correction.

We now turn to discussing the Feynman diagrams building the amplitudes $A_{gg \rightarrow Hq\bar{q}}^{(2,0)}$, $A_{gg \rightarrow Hq\bar{q}}^{(0,2)}$, $A_{gq \rightarrow Hq}^{(1,0)}$ and $A_{gq \rightarrow Hq}^{(-1,2)}$ that contribute to the cross sections presented in this work.

The amplitude $A_{gg \rightarrow Hq\bar{q}}^{(2,0)}$ is built from the diagrams depicted in Fig. 1 where the Higgs is produced via weak vector boson fusion and interfered with the leading QCD gluon-fusion diagrams shown in Fig. 3.

Diagrams of the class 1d and 1e, where the Higgs is produced via gluon-fusion, feature a Z-boson propagator² which however does not yield any Breit-Wigner resonance as they are interfered against the QCD diagrams of Fig. 3. We must nonetheless regulate the Z-

²The diagram analogous to 1e with a photon instead of the Z-boson is exactly zero in virtue of Furry's theorem.

boson propagator pole, which motivates our use in this computation of the complex-mass scheme [11, 12] with finite widths for the internal top quark and unstable weak gauge bosons. These diagrams 1d and 1e are however ignored when considering their squared contribution to $\sigma_{pp \rightarrow H+X}^{(1,1)}$, since in this case they are best accounted for in the narrow-width approximation as the LO prediction for associated Higgs production, *i.e.* $\sigma_{gg \rightarrow HZ}^{(1,1)}$ (also reported in this work).

Finally, diagrams of the class 1f are specific to the third-generation quarks where the Higgs can also be emitted from the top-quark running in the loop. This contribution is analogous to that of the heavy quarks in the two-loop electroweak corrections to Higgs production investigated in ref. [13] and, for this reason, we found it interesting to report our results separately for the processes $gg \rightarrow Hq\bar{q}$, with $q \equiv u, d, c, s$, and $gg \rightarrow b\bar{b}H$.

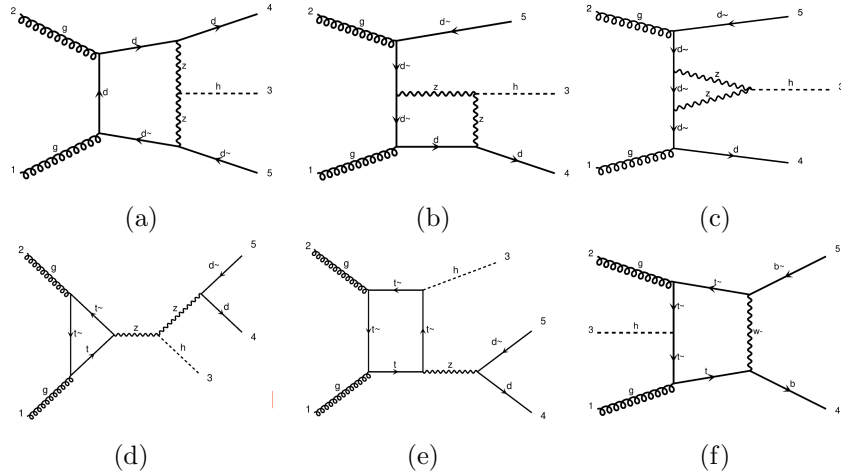


Figure 1: Representative subset of diagrams contributing to the amplitude $A_{gg \rightarrow Hq\bar{q}}^{(0,2)}$. In diagrams 1a, 1b and 1c, the Z boson can be interchanged with a W boson. Diagrams 1d and 1e are contributions to the production of a Higgs in association with a Z boson and are only included in the computation of $\sigma_{pp \rightarrow H+X}^{(1,1)}$, and not that of $\sigma_{pp \rightarrow H+X}^{(1,2)}$. Diagrams of the class 1f are only present for the process $gg \rightarrow Hb\bar{b}$.

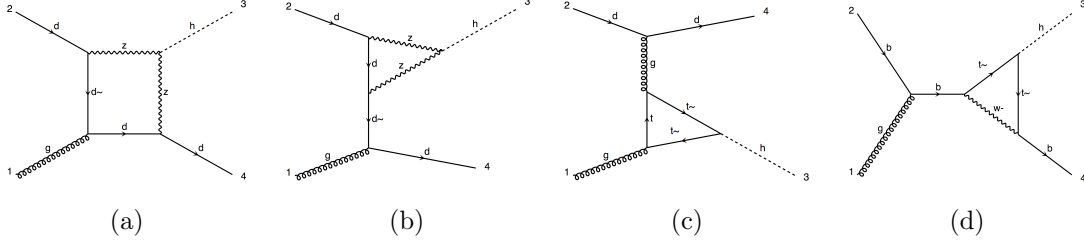


Figure 2: Diagrammatic contributions to the amplitudes $A_{gq \rightarrow Hq}^{(-1,2)}$ (Figs. 2a, 2b, 2d) and $A_{gq \rightarrow Hq}^{(1,0)}$ (Fig. 2c), yielding $\sigma_{gq \rightarrow Hq}^{(-1,2)}$ and $\sigma_{gq \rightarrow Hq}^{(0,2)}$ respectively. Diagrams 2a and 2b also appear in the reduced matrix elements factorised by the collinear subtraction local counterterms of Eqs. 3.2 and 3.1. Notice that diagrams belonging to the class 2d are specific to the process $gb \rightarrow Hb$. In all cases, the full top-quark mass dependence is retained.

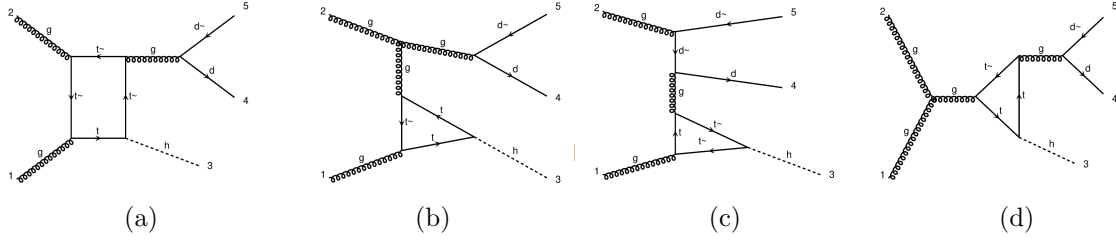


Figure 3: Diagrams building the amplitude $A_{gg \rightarrow Hq\bar{q}}^{(2,0)}$ against which the diagrams listed in Fig. 1 are interfered to yield $\sigma_{gg \rightarrow Hq\bar{q}}^{(1,1)}$. The full top-quark mass dependence is retained.

3 Initial-state collinear singularities

All of the one-loop amplitudes considered in this paper are free of explicit ultraviolet and infrared divergences that can arise from the integration over the loop momenta. In other words, working in dimensional regularisation with $D \equiv 4 - 2\epsilon$, their analytic expressions do not contain explicit poles in the dimensional regulator ϵ . However, matrix elements may feature non-integrable infrared divergences in regions of the phase space which correspond to unresolved configurations. In order to discuss this issue, we concentrate on the amplitude $A_{gg \rightarrow Hq\bar{q}}^{(0,2)}$ as it constitutes the main focus of the present work.

In principle, the process $gg \rightarrow Hq\bar{q}$ presents infrared divergences when the quark-antiquark pair in the final state is collectively soft, and/or when one or both of the quarks are collinear to the direction of an incoming gluon. However, thanks to the factorisation properties of QCD, in double-unresolved configurations the amplitude $A_{gg \rightarrow Hq\bar{q}}^{(0,2)}$ can be approximated by universal factors times the reduced amplitude $A_{q\bar{q} \rightarrow H}^{(-2,2)}$ (that is, of order g^3) which is identically zero. Indeed, the triangle one-loop diagrams for $q\bar{q} \rightarrow H$ require a mass insertion for the chirality flip and therefore vanishes for massless onshell quarks. This explains why the interference involving the amplitude $A_{gg \rightarrow Hq\bar{q}}^{(0,2)}$ only requires the subtraction of *single*-unresolved infrared

limits, while the interference built upon the amplitude $A_{gq \rightarrow Hq}^{(-1,2)}$ does not require IR subtraction at all.

The same observations can be made, perhaps more intuitively, by inspecting the representative Feynman diagrams depicted in Fig. 1. It is straightforward to see that propagators of massless partons which do not belong to closed loops can go on-shell only in the graphs of type 1b and 1c. In the case of the diagram 1b, this happens when antiquark \bar{d}_5 becomes collinear to gluon g_2 such that the hard scattering subgraph corresponds to diagram 2a. By contrast, in the kinematic limit where quark d_4 is collinear to gluon g_1 and quark \bar{d}_5 is collinear to gluon g_2 , both non-loop propagators of graph 1c are singular. The subgraph that describes the hard scattering process, however, evaluates to zero for massless quarks as explained before, thus avoiding the singularity. In the limit where only one of the quarks is collinear to an incoming gluon, the hard part of diagram 1c matches that of graph 2b.

From the observations drawn so far, we conclude that for the local subtraction of implicit singularities it is sufficient to consider standard NLO initial-collinear counterterms. These subtraction terms are to be added back, analytically integrated over the unresolved degrees of freedom yielding explicit poles in the dimensional regulator ϵ . These poles cancel against those part of the PDF renormalisation counterterms, as guaranteed by collinear beam factorisation, thus rendering the complete computation finite.

The formal expression which describes this subtraction procedure and the combination with PDF renormalisation counterterms reads:

$$\sigma_{gg \rightarrow Hq\bar{q}}^{(m,n)} = \int_0^1 dx_1 \int_0^1 dx_2 f_g(x_1) f_g(x_2) \left\{ \int d\Phi_{Hq\bar{q}} \left[\mathcal{M}_{gg \rightarrow Hq\bar{q}}^{(m,n)} \mathbf{J}(\phi_{Hq\bar{q}}) - \sum_{\pi} \mathbf{C}_{gq} \otimes \mathcal{M}_{gq \rightarrow Hq}^{(m-1,n)} \mathbf{J}(\tilde{\phi}_{Hq}) \right] \right. \quad (3.1)$$

$$\left. + \sum_{\pi} \int d\Phi_{Hq} \int_0^1 d\xi [\langle \mathbf{C}_{gq} \rangle(\xi) + \Delta_{gq}(\xi)] \mathcal{M}_{gq \rightarrow Hq}^{(m-1,n)} \mathbf{J}(\phi_{Hq}) \right\}, \quad (3.2)$$

where the dependences on the factorisation and renormalisation scales μ_F and μ_R as well as on the kinematic inputs for the matrix elements have been suppressed for brevity. The sums run over the four permutations π that are obtained exchanging the quark and the antiquark in the final state and/or the two initial-state gluons among themselves. The symbol \mathbf{C}_{ij} denotes the local counterterm for particles i and j going collinear and $\langle \mathbf{C}_{ij} \rangle$ its counterpart analytically integrated over the unresolved degrees of freedom. The observable functions are indicated with \mathbf{J} , and Δ_{ik} is the PDF renormalisation kernel for parton with flavour i to change into species k before entering the hard process. The notation $\tilde{\phi}_{Hq}$ indicates reduced kinematics of lower multiplicity which are obtained by mapping a pair of collinear partons to a massless parent. The concrete expressions of all subtraction ingredients closely follow ref. [14] and are presented more explicitly in appendix A, where we also explicitly show that our subtraction counterterms correctly regulate the relevant collinear singularities.

4 Setup of the computation and numerical results

The amplitudes $A_{gg \rightarrow Hq\bar{q}}^{(0,2)}$ and $A_{gq \rightarrow Hq}^{(-1,2)}$ that factorise a Higgs coupling to weak bosons were first computed analytically (for massless quarks only) in ref. [15], in the different context of NLO QCD corrections to weak vector-boson fusion. In the present case and as indicated in Table 1, in order to obtain contributions to $\sigma_{gg \rightarrow Hq\bar{q}}^{(1,1)}$ and $\sigma_{gq \rightarrow Hq}^{(0,1)}$, these amplitudes must be interfered against their corresponding QCD analog.

Nowadays such one-loop amplitudes are readily available from many automated one-loop matrix-element generators. However, a high degree of flexibility is necessary in order to be able to select the relevant diagrams and interferences, and to construct the appropriate subtraction terms. This motivates our choice of generating the relevant one-loop squared amplitudes using MADLOOP [16], part of MADGRAPH5_AMC@NLO [17] (henceforth abbreviated MG5AMC), as it can efficiently generate and interfere [18] arbitrary one-loop amplitudes in the SM and beyond. MADLOOP uses NINJA [19,20] and ONELOOP [21], or alternatively COLLIER [22], for performing one-loop reductions and for the evaluation of the scalar one-loop master integrals. We present in appendix C some details about the generation procedure as well as benchmark numbers in order to facilitate the reproduction of our results. Moreover, we have cross-checked MADLOOP’s numerical implementation of the amplitudes $A_{gg \rightarrow Hq\bar{q}}^{(2,0)}$ and $A_{gq \rightarrow Hq\bar{q}}^{(0,2)}$ against a completely independent and analytical computation described in appendix B.

As already mentioned, we choose to renormalise all unstable particles in the complex-mass scheme [11,12] and consider the SM input parameters given in Table 2.

Parameter	value	Parameter	value	Parameter	value
PDF set	PDF4LHC15_nlo_30	$\mu_R = \mu_F$	$M_H/2, M_H$	M_t	174.3
$\alpha_S(m_Z^2)$	from PDF set	G_F	$\frac{\pi\alpha}{\sqrt{2}m_W^2(1-m_W^2/m_Z^2)}$	Γ_t	1.35408
$\sqrt{\hat{s}}$	13000	α^{-1}	132.507	$\frac{y_tv}{\sqrt{2}}$	m_t
\bar{M}_Z	91.188	$\bar{\Gamma}_Z$	2.42823	M_b	0.0
\bar{M}_W	80.419	$\bar{\Gamma}_W$	2.02844	$\frac{y_bv}{\sqrt{2}}$	0.0
M_H	125.0	Γ_H	0.0	V_{ij}^{CKM}	δ_{ij}

Table 2: SM parameters used for obtaining all numerical results presented in Table 3. Dimensionful parameters are given in GeV. Lower-case mass parameters correspond to their complex-valued counterpart in the complex-mass scheme, *i.e.* $m_W = \sqrt{\bar{M}_W^2 - i\bar{\Gamma}_W\bar{M}_W}$.

The numerical Monte-Carlo integration as well as the necessary IR subtraction procedure, presented in Eqs. 3.1 and 3.2 as well as in appendix A, have been implemented in a private

extension of MG5AMC currently under development. The poles in the dimensional regulator ϵ have been checked to cancel as expected.³ Moreover, we have validated our code by comparing NLO QCD cross sections against results from MG5AMC for the processes $pp \rightarrow Z$ and $pp \rightarrow H$, the latter in the Higgs Effective Theory.

Our results are presented in Table 3. Along with the different contributions to the inclusive cross section for Higgs production, we also report the semi-inclusive cross sections for the production of a Higgs boson with transverse momentum larger than 400 GeV. The motivation to consider this boosted Higgs regime is twofold. On one side, it mimics typical experimental selection cuts used to reduce backgrounds and study new physics effect prominent in that regime. On the other side, it selects a region of phase space where real emissions are typically hard and the relative importance of the corrections computed in this work may in principle be enhanced.

We find that the squared contributions of order $\mathcal{O}(\alpha_s^2 \alpha^3)$ can be suppressed compared to their $\mathcal{O}(\alpha_s^3 \alpha^2)$ counterpart by less than what is expected by their parametric ratio α/α_s . This is for example the case for the processes involving b quarks, and it can be explained by the kinematic suppressions interfering contributions are typically subject to.

Also, contributions of order $\mathcal{O}(\alpha_s^m \alpha^n)$ with $m+n=4$ are numerically more relevant than those with $m+n=5$ in spite of their suppression by one quark luminosity. The quark-initiated weak corrections are however still small in comparison with the whole $\sigma_{pp \rightarrow H+X}^{(\alpha_s^3 \alpha^2)}$, and can thus be safely neglected as already observed in ref. [23]. These two observations reinforce the conclusion that the contributions to $\sigma_{gg \rightarrow Hq\bar{q}}^{(\alpha_s^3 \alpha^2)}$ that are computed in this work and which have been neglected up to this point are of similar (ir)relevance to that of other neglected terms of weak origin.

The cross section $\sigma_{gg \rightarrow Hb\bar{b}}^{(\alpha_s^3 \alpha^2)}$ from only final-state b quarks reveals that contributions featuring Higgs production from the internal top quark line (see Fig. 1f) are comparable and of opposite sign to that of emissions from internal weak bosons. This fact contrasts with the study of ref. [13] of the two-loop amplitude $A_{gg \rightarrow H}^{(0,2)}$ where it was instead found that Higgs emissions from internal top quarks only contribute to less than 2% of the complete amplitude at this order, and could thus be safely ignored in the computation of the three-loop amplitude $A_{gg \rightarrow H}^{(2,2)}$ of refs. [8–10]. Indeed, the higher partonic collision energy probed by $A_{gg \rightarrow Hb\bar{b}}^{(1,2)}$ enhances contributions from internal top-quark Higgs emissions, even more so in the boosted regime. Similarly, the same mechanism enables the bottom-quark initiated contribution $\sigma_{bg \rightarrow Hb}^{(\alpha_s^2 \alpha^2)}$ at the same level as that of the channels initiated by each other valence quark flavour.

The squared contribution $\sigma_{gg \rightarrow Hb\bar{b}}^{(\alpha_s^2 \alpha^3, \text{no-HZ})}$ omits the diagrams 1d and 1e featuring a Z boson

³This check of course only considers the convoluted term of Eq. 3.2 as our computation involves no virtual contribution. Also, for the pole cancellation to occur, it is important to restrict the initial state contributions to gluons only, as poles from the beam factorisation terms Δ_{qg} and Δ_{qq} remain uncanceled given that we ignore the corresponding real-emission subprocesses.

cross section interferences	[fb]	cross section squared amplitudes	[fb]
$\sigma_{gg \rightarrow Hq\bar{q}}^{(\alpha_s^3 \alpha^2)}$	11.93 \pm 0.04	$\sigma_{gg \rightarrow Hq\bar{q}}^{(\alpha_s^2 \alpha^3, \text{no-HZ})}$	-0.260 \pm 0.004
	13.31 \pm 0.08		-2.135 \pm 0.003
$\sigma_{gg \rightarrow Hb\bar{b}}^{(\alpha_s^3 \alpha^2)}$	-5.94 \pm 0.03	$\sigma_{gg \rightarrow Hb\bar{b}}^{(\alpha_s^2 \alpha^3, \text{no-HZ})}$	3.867 \pm 0.008
	-7.36 \pm 0.03		0.882 \pm 0.006
$\sigma_{qg \rightarrow Hq}^{(\alpha_s^2 \alpha^2)} + \sigma_{\bar{q}g \rightarrow H\bar{q}}^{(\alpha_s^2 \alpha^2)}$	-163.9 \pm 0.1	$\sigma_{qg \rightarrow Hq}^{(\alpha_s \alpha^3)} + \sigma_{\bar{q}g \rightarrow H\bar{q}}^{(\alpha_s \alpha^3)}$	52.3 \pm 0.2
	-137.0 \pm 0.2		48.6 \pm 0.1
$\sigma_{bg \rightarrow Hb}^{(\alpha_s^2 \alpha^2)} + \sigma_{\bar{b}g \rightarrow H\bar{b}}^{(\alpha_s^2 \alpha^2)}$	20.95 \pm 0.04	$\sigma_{bg \rightarrow Hb}^{(\alpha_s \alpha^3)} + \sigma_{\bar{b}g \rightarrow H\bar{b}}^{(\alpha_s \alpha^3)}$	13.78 \pm 0.05
	19.45 \pm 0.06		13.82 \pm 0.02
$\sigma_{\text{interf.}+\text{squared}}^{\text{total}}$	30.9 \pm 0.2	$\sigma_{gg \rightarrow HZ}^{(\alpha_s^2 \alpha^2, \bar{\Gamma}_Z=0)}$	98.17 \pm 0.05
	24.9 \pm 0.2		76.27 \pm 0.03

$p_T(H) > 400 \text{ GeV}$

$\sigma_{gg \rightarrow Hq\bar{q}}^{(\alpha_s^3 \alpha^2)}$	-0.0054 \pm 0.0002	$\sigma_{gg \rightarrow Hq\bar{q}}^{(\alpha_s^2 \alpha^3, \text{no-HZ})}$	0.00390 \pm 0.00003
	0.00674 \pm 0.00008		0.00154 \pm 0.00004
$\sigma_{gg \rightarrow Hb\bar{b}}^{(\alpha_s^3 \alpha^2)}$	-0.0093 \pm 0.0002	$\sigma_{gg \rightarrow Hb\bar{b}}^{(\alpha_s^2 \alpha^3, \text{no-HZ})}$	0.0363 \pm 0.0003
	-0.00197 \pm 0.00009		0.0118 \pm 0.0002
$\sigma_{qg \rightarrow Hq}^{(\alpha_s^2 \alpha^2)} + \sigma_{\bar{q}g \rightarrow H\bar{q}}^{(\alpha_s^2 \alpha^2)}$	-1.005 \pm 0.003	$\sigma_{qg \rightarrow Hq}^{(\alpha_s \alpha^3)} + \sigma_{\bar{q}g \rightarrow H\bar{q}}^{(\alpha_s \alpha^3)}$	0.1019 \pm 0.0002
	-0.7486 \pm 0.0005		0.0841 \pm 0.0001
$\sigma_{bg \rightarrow Hb}^{(\alpha_s^2 \alpha^2)} + \sigma_{\bar{b}g \rightarrow H\bar{b}}^{(\alpha_s^2 \alpha^2)}$	-0.0326 \pm 0.0001	$\sigma_{bg \rightarrow Hb}^{(\alpha_s \alpha^3)} + \sigma_{\bar{b}g \rightarrow H\bar{b}}^{(\alpha_s \alpha^3)}$	0.1033 \pm 0.0003
	-0.0268 \pm 0.00003		0.0950 \pm 0.0002
$\sigma_{\text{interf.}+\text{squared}}^{\text{total}}$	-0.502 \pm 0.003	$\sigma_{gg \rightarrow HZ}^{(\alpha_s^2 \alpha^2, \bar{\Gamma}_Z=0)}$	0.3049 \pm 0.0006
	-0.3615 \pm 0.0008		0.2159 \pm 0.0003

Table 3: Fully and semi inclusive cross sections obtained with SM input parameters given in Table 2 for the processes $gg \rightarrow Hq\bar{q}$ and $gg \rightarrow Hb\bar{b}$, as (partial) contributions to the corrections of order $\mathcal{O}(\alpha_s^3 \alpha^2)$ and $\mathcal{O}(\alpha_s^2 \alpha^3)$ to inclusive Higgs production. For the contributions of order $\mathcal{O}(\alpha_s^2 \alpha^3)$ labelled “no-HZ”, the diagrams of the class 1d and 1e are ignored, as they are best accounted for in the narrow-width approximation as the LO contribution to the process $gg \rightarrow HZ$, which is also shown. We also report the $\mathcal{O}(\alpha_s^2 \alpha^2)$ and $\mathcal{O}(\alpha_s \alpha^3)$ contributions from the quark-initiated processes $qg \rightarrow Hq$ and $bg \rightarrow Hb$. Finally, we consider the boosted regime, in which the Higgs transverse momentum is required to be at least 400 GeV. In each bracket separated by a dashed line, the upper number corresponds to the scale choice $\mu_R = \mu_F = m_H/2$ while the lower one corresponds to $\mu_R = \mu_F = m_H$.

decay since it is best accounted for in the narrow-width approximation. It is however clear that the extent to which one should consider Higgs production in association with an on-shell Z boson depends on the particular observable considered. We chose to report here the quantity $\sigma_{gg \rightarrow HZ}^{(\alpha_s^2 \alpha^2, \bar{\Gamma}_Z=0)}$ only to serve as an upper bound to this contribution.

Notice that the contribution $\sigma_{gg \rightarrow Hq\bar{q}}^{(\alpha_s^2 \alpha^3, \text{no-HZ})}$ is negative, despite involving squared amplitudes. This originates from the finite logarithms in the PDF renormalisation term Δ_{gq} and integrated counterterm $\langle \mathbf{C}_{gq} \rangle$, stemming from dimensional regularisation. Our results also highlight that considering a subset of higher-order corrections and factorising only a particular combination of initial-state flavours typically yields a large dependence on the factorisation scale. This is especially true for squared amplitude contributions and the boosted regime, for which the chosen fixed scales proportional to the Higgs mass (as it is tailored to the prediction of the inclusive Higgs production cross section) are not well suited in light of the significantly larger collision energies probed. We choose to report here *absolute* factorisation scale dependency, given that some contributions can be accidentally close to zero⁴ for one of the two scale choices. A more detailed analysis of the sensitivity of these contributions to the factorisation scale is beyond the scope of this work.

The overall magnitude of all contributions computed here is such that they can be safely neglected in light of the total size of mixed QCD-weak corrections, which is estimated to be of the order of 2 pb with an associated uncertainty in the range of 200 fb [9, 10]. The aggregated sum σ_{total} of all contributions computed in this work is only meant to serve as qualitative highlight of that fact. Our results then further support the factorisation approximation when accounting for mixed weak and QCD corrections to inclusive Higgs production.

The hierarchy of the various terms is altered when considering the boosted Higgs regime, where the kinematic suppression of gluon-initiated interference contributions is strong enough to make them of the same order or smaller than their squared counterpart. All interference contributions also become negative in this case, while the square term $\sigma_{gg \rightarrow Hq\bar{q}}^{(\alpha_s^2 \alpha^3, \text{no-ZH})}$ is now positive as hard real emissions become dominant. Overall, none of the contributions computed plays a significant role in that scenario either, given that the pure QCD contribution is estimated in ref. [24] to be 25 fb with a large theoretical uncertainty exceeding 20%.

5 Conclusion

The large QCD corrections to inclusive Higgs production at LHC13 calls for accounting for mixed weak and QCD corrections in a multiplicative scheme, that is assuming their complete factorisation. In light of the accuracy sought-after for this process, it is important to assess

⁴This is for example the case in $\sigma_{gg \rightarrow Hb\bar{b}}^{(\alpha_s^2 \alpha^3, \text{no-ZH})}|_{\mu_F=m_H}$ where Higgs emissions from weak bosons are close to equal and opposite in sign to emissions from internal top-quarks, and in $\sigma_{gg \rightarrow Hq\bar{q}}^{(\alpha_s^2 \alpha^3, \text{no-ZH})}|_{\mu_F=m_H/2}$ where the cancellation occurs between the hard reals and the logarithms in ξ part of the integrated counterterms $\langle \mathbf{C}_{gq} \rangle$.

the validity of this factorisation assumption by explicitly computing $\sigma_{pp \rightarrow H+X}^{(1,1)}$, namely the mixed QCD and weak correction of order $\mathcal{O}(\alpha_s^3 \alpha^2)$ to the Higgs inclusive cross section.

To this end, two groups [8–10] computed $\sigma_{gg \rightarrow H+X}^{(1,1)}$ and found that it supports the hypothesis that weak corrections factorise. These works however neglected the quark-initiated components as well as the “double-real” channel $gg \rightarrow Hq\bar{q}$ and we confirm here that these terms can be safely neglected, amounting to about 5% of the total mixed weak and QCD corrections. We verified that our conclusions also apply when imposing that the Higgs transverse momentum lies above 400 GeV. The interference nature of the contributions $\sigma_{gg \rightarrow Hq\bar{q}}^{(1,1)}$ and $\sigma_{gq \rightarrow Hq}^{(1,1)}$ renders them prone to kinematic suppressions, and we indeed found that the square of the one-loop weak amplitudes involved can be larger than naively expected from their parametric suppression of α/α_s . The selective nature of the contributions computed in this work is such that they feature a large factorisation scale dependency, further stressing that their inclusion would require to also consider *all* other partonic channels.

Besides further establishing the validity of the hypothesis assumed when accounting for weak corrections to inclusive Higgs production, our work also showcases the novel flexibility brought by recent developments in the realm of automated one-loop matrix element generation and Monte-Carlo integration for higher-order computations.

Acknowledgments

We are greatly indebted to C. Anastasiou, V. del Duca, N. Deutschmann, E. Furlan, B. Mistlberger and C. Specchia for fruitful discussions. This project has received funding from the European Research Council (ERC) under grant agreements No 772099 (JetDynamics) and No 694712 (PertQCD). We thank the Galileo Galilei Institute for Theoretical Physics for the hospitality and the INFN for partial support during the completion of this work.

Appendix A Initial-collinear counterterms

In this appendix, we detail all ingredients that are necessary for the subtraction of implicit singularities outlined in Eqs. 3.1–3.2, and we demonstrate that the matrix element for $g_1 g_2 \rightarrow q_3 \bar{q}_4 H_5$ is correctly regulated in the regions of phase space close to unresolved configurations. As already announced in Section 3, the construction and notation follow closely ref. [14].

Let us begin with the expression of the local initial-collinear counterterms in Eq. 3.1. In general, in order for these counterterms to approximate the matrix element point by point in the phase space, spin correlations need to be taken into account. Suppressing the coupling orders, we define

$$[\mathbf{C}_{g_1 q_3} \otimes \mathcal{M}_{\bar{q}_{13} g_2 \rightarrow \bar{q}_4 H_5}](\phi_{q_3 \bar{q}_4 H_5}) \equiv (8\pi\alpha_s \mu^{2\epsilon}) \frac{1}{s_{g_1 q_3}} \hat{P}_{g_1 q_3}^{ss'}(1/z) \frac{\omega(\bar{q}_{13})}{\omega(g_1)} \times \mathcal{M}_{\bar{q}_{13} g_2 \rightarrow \bar{q}_4 H_5}^{ss'}(\tilde{\phi}_{\bar{q}_4 H_5}) \theta(y_0 - y), \quad (\text{A.1})$$

where s and s' respectively specify the spin of the quark which enters the reduced amplitude and the corresponding conjugate. The factor $\omega(\bar{q})/\omega(g)$ accounts for the different averaging on the initial state spins and colours in the matrix elements and equals $N_c/(N_c^2 - 1)$ in four spacetime dimensions. The symbol $\hat{P}_{gq}^{ss'}$ denotes the final-final qg splitting function

$$\hat{P}_{gq}^{ss'}(z) \equiv \delta^{ss'} C_F \left[\frac{1 + (1 - z)^2}{z} - \epsilon z \right], \quad (\text{A.2})$$

and the variable z in Eq. A.1 is computed using

$$z \equiv \frac{Q \cdot (p_1 - p_3)}{Q \cdot p_1}, \quad (\text{A.3})$$

with $Q = p_1 + p_2$. For the process at hand, since the parton which enters the hard process after the splitting is always a quark, spin correlations are absent as indicated by $\delta^{ss'}$ in Eq. A.2. The momentum mapping that we use to determine the reduced phase-space point $\tilde{\phi}_{qH}$ is the one used for two initial-state partons in Catani–Seymour dipole subtraction (see Section 5.5 of [25]).⁵ Finally, the Heaviside θ function at the end of Eq. A.1 controls the region of phase-space where the counterterm is active through the parameter y_0 , which determines the range for the variable $y \equiv 2p_1 \cdot p_3/Q^2$.

At this point, all the elements needed to check that Eq. (3.1) only features integrable singularities have been presented. In order to validate our subtraction and assess the numerical stability of the integrand which is built from the interference of two one-loop amplitudes, we start from a random resolved kinematic configuration and examine the behaviour as different collinear limits are approached. We control the distance from any given unresolved limit using a scaling variable λ , which is engineered to approach the singular configuration at a pace such

⁵ Note that this mapping involves recoiling against all final state particles, and it would not be efficient for studying differential Higgs observables.

that the phase-space volume between λ and $\lambda + d\lambda$ is proportional to λ itself. For a kinematic configuration with a centre-of-mass energy of 1 TeV and in the case of a collinear pair, the typical invariant mass is then $\mathcal{O}(1 \text{ GeV})$ for $\lambda = 10^{-6}$ and $\mathcal{O}(1 \text{ MeV})$ for $\lambda = 10^{-12}$. Under the same conditions and in the case of two collinear pairs, the typical invariant mass of each of them is $\mathcal{O}(1 \text{ GeV})$ for $\lambda = 10^{-12}$ and $\mathcal{O}(1 \text{ MeV})$ for $\lambda = 10^{-24}$ instead. For the sake of concreteness, we consider the partonic subprocess $g_1 g_2 \rightarrow b_3 \bar{b}_4 H_5$, with the understanding that all qualitative features are identical in the case of light quark flavours in the final state.

In Fig. 4, we display the behaviour of the matrix element interference and its four initial-collinear counterterms as a function of λ for a given starting kinematic configuration. The left panels simply show the ratio of counterterms to the matrix element. In the right panels, we plot their sum weighted by λ , which is representative of the contribution to the total integral coming from a neighbourhood of λ . We therefore expect the integral to be convergent if this quantity tends to zero when $\lambda \rightarrow 0$. In Fig. 4a we consider the limit $C(1, 3)$, where the matrix element is approximated by the counterterm $C(1, 3)$ and all other terms in the sum over π of Eq. (3.1) are regular. The cases of $C(2, 4)$, $C(1, 4)$ and $C(2, 3)$ are fully analogous. In Fig. 4b we study the limit of two collinear pairs $C(1, 3)C(2, 4)$ which, as discussed in Section 3, does not require any additional treatment since the matrix element for $q\bar{q} \rightarrow H$ at order $\mathcal{O}(g_s g^2)$ is zero. Finally, in Fig. 4c we consider the limit $C(3, 4)$ to confirm that the matrix element of order $\mathcal{O}(\alpha_s^2 \alpha^2)$ for $gg \rightarrow b\bar{b}H$ does not feature a non-integrable divergence when the two quarks in the final state are collinear. We note that the figures in this section can be sensitive to the numerical stability parameters of MADLOOP which, among other things, control when to switch to a slower quadruple precision evaluation. Further discussion of this technical aspect is however beyond the scope of this work and we limit ourselves to reporting here that all Monte-Carlo integrations performed in this work could be successfully carried out using MADLOOP's default parameters⁶. Incidentally, we observe that in order to obtain results at the level of precision needed for this work it is not necessary to introduce a technical cutoff.

The integral of the collinear counterterm over the unresolved phase space has been computed in [14] and reads

$$\begin{aligned} \langle \mathbf{C}_{gq} \rangle(\xi) = \frac{\alpha_s}{2\pi} S_\epsilon \left[\frac{\mu_R^2}{Q^2} \right]^\epsilon \frac{T_R}{C_F} \left\{ [\xi^2 + (1 - \xi)^2] \left[-\frac{1}{\epsilon} + \ln(1 - \xi)(1 + \theta[\xi - (1 - y_0)]) \right] \right. \\ \left. + \ln(y_0)\theta[(1 - y_0) - \xi] + 2\xi(1 - \xi) \right\} + \mathcal{O}(\epsilon), \quad (\text{A.4}) \end{aligned}$$

where $Q = p_1 + p_2$ for the *reduced* process $g_1 q_2 \rightarrow q_3 H_4$ and we have defined

$$S_\epsilon \equiv \frac{(4\pi)^\epsilon}{\Gamma(1 - \epsilon)}. \quad (\text{A.5})$$

⁶We note however that it proved to be necessary to employ an estimate of MADLOOP's accuracy based on the comparison of two separate numerical evaluations that differ by a Lorentz transformation of the kinematic inputs (by setting MADLOOP's parameter `NRotations.DP` to 1).

The explicit pole in the dimensional regulator ϵ featured by this integrated counterterm is cancelled by the contribution from PDF renormalisation, which is given by

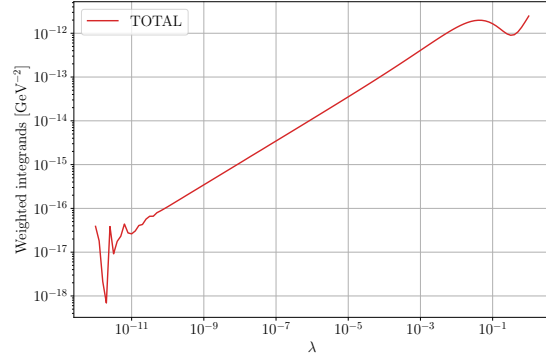
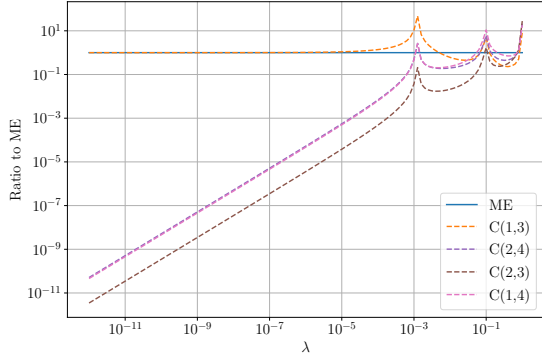
$$\Delta_{gq}(\xi) = \frac{\alpha_s}{2\pi} S_\epsilon \frac{1}{\epsilon} \left[\frac{\mu_R^2}{\mu_F^2} \right]^\epsilon P_{gq}(\xi), \quad (\text{A.6})$$

where the relevant Altarelli–Parisi splitting kernel reads ⁷

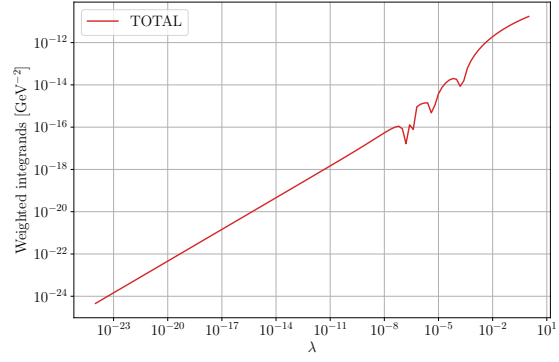
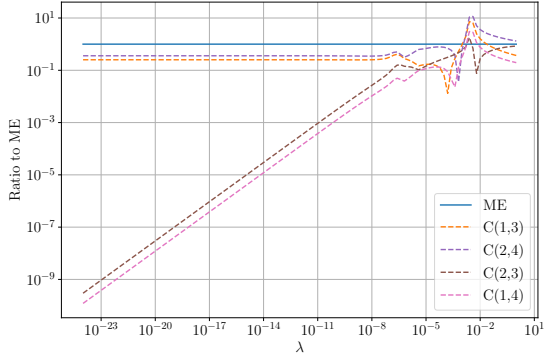
$$P_{gq}(\xi) = T_R[\xi^2 + (1 - \xi)^2]. \quad (\text{A.7})$$

We have confirmed that in our implementation of this subtraction scheme the sum of (3.1) and (3.2) does not depend on y_0 , which provides a non-trivial cross-check of $\mathcal{O}(\epsilon^0)$ terms.

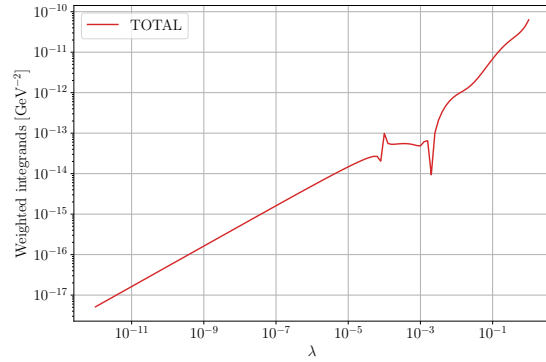
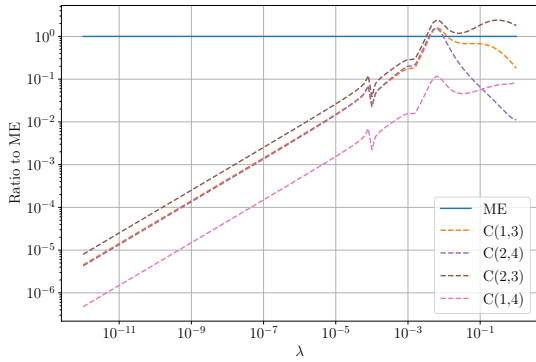
⁷ Note that in our notation the first subscript indicates the parton extracted from the hadron according to its PDF, and the second one denotes the parton that enters the hard process.



(a) $C(1,3)$ limit



(b) $C(1,3)C(2,4)$ limit



(c) $C(3,4)$ limit

Figure 4: Behaviour of the terms in Eq. 3.1 for the process $g_1 g_2 \rightarrow b_3 \bar{b}_4 H_5$ when approaching different unresolved limits. See text for details.

Appendix B Analytical computation of the amplitudes $A_{gg \rightarrow Hq\bar{q}}^{(2,0)}$ and $A_{gg \rightarrow Hq\bar{q}}^{(0,2)}$

The analytic validation is performed by computing the form factors for the QCD background depicted in the diagrams Fig. 3 and the weak contributions with sample diagrams shown in Figs. 1a to 1c. While we retain the full quark mass dependence for the QCD background, we assume massless quarks for the weak contributions. The computation is performed in $D = 4 - 2\epsilon$ dimensions. However, due to the special reduction of the scalar pentagon integrals, the final result is only valid for the provided order $\mathcal{O}(\epsilon^0)$ in the dimensional regulator (see Sec. B.2).

The amplitude for the weak process $g_1 g_2 \rightarrow q_3 \bar{q}_4 H_5$ may be written in the general form

$$A_{gg \rightarrow q\bar{q}H}^{(0,2)} = A_{gg \rightarrow q\bar{q}H}^{(0,2),VV} + A_{gg \rightarrow q\bar{q}H}^{(0,2),AV} + A_{gg \rightarrow q\bar{q}H}^{(0,2),VA} + A_{gg \rightarrow q\bar{q}H}^{(0,2),AA} \quad (\text{B.1})$$

$$= \varepsilon_{\mu_1}(p_1) \varepsilon_{\mu_2}(p_2) \bar{u}^{s_3}(p_3) v^{s_4}(p_4) \mathcal{F}_{s_3 s_4}^{\mu_1 \mu_2}, \quad (\text{B.2})$$

where in the following we will denote the form factor by $\mathcal{F}^{\mu_1 \mu_2}$, suppressing the spinor indices. We separate couplings of the quarks to the weak gauge bosons according to

$$udW^+ \propto g_V \gamma^\mu + g_A \gamma^\mu \gamma^5, \quad udW^- \propto g_V^* \gamma^\mu + g_A^* \gamma^\mu \gamma^5 \quad \text{and} \quad (\text{B.3})$$

$$qqZ \propto g_V \gamma^\mu + g_A \gamma^\mu \gamma^5, \quad (\text{B.4})$$

and refer to g_V as the vector and to g_A as the axial coupling constant. In the following, we restrict ourselves to the case of d quarks in the final state for concreteness. We will first discuss the computation of $A_{gg \rightarrow d\bar{d}H}^{(0,2),VV} \propto |g_V|^2$ and then argue that this piece is sufficient to determine the complete amplitude.

In order to compute the form factors, we first generate all contributing diagrams with QGRAF [26] and perform the color-, Dirac- and Lorentz algebra in Mathematica, whereas the γ traces are performed using FORM [27]. For more compact expressions, we choose an axial gauge for the external gluons g_1 and g_2 , such that

$$p_1 \cdot \varepsilon_1(p_1) = 0 \quad p_2 \cdot \varepsilon_1(p_1) = 0 \quad p_2 \cdot \varepsilon_2(p_2) = 0 \quad p_1 \cdot \varepsilon_1(p_2) = 0, \quad (\text{B.5})$$

with the physical polarization sum

$$\sum_{\text{polarization}} \varepsilon_\mu^*(p_i) \varepsilon_\nu(p_i) = -g_{\mu\nu} + \frac{p_{1\mu} p_{2\nu} + p_{2\mu} p_{1\nu}}{p_1 \cdot p_2} \quad \text{for } i = 1, 2. \quad (\text{B.6})$$

As a direct consequence of the gauge choice, terms in the form factors proportional to $p_1^{\mu_1}$, $p_2^{\mu_1}$, $p_1^{\mu_2}$ or $p_2^{\mu_2}$ can be set to zero, since they will not contribute to the amplitude. Internal gauge bosons and quarks are treated in the Feynman gauge.

B.1 Tensor reduction to scalar integrals

The form factor $\mathcal{F}^{\mu_1\mu_2}$ can be written as

$$\mathcal{F}^{\mu_1\mu_2} = \sum_i \alpha_i \mathcal{S}_i^{\mu_1\mu_2} = \sum_i \alpha_i \int \frac{N^{\mu_1\mu_2}(k)}{D_1 \dots D_{m_i}} d^D k, \quad (\text{B.7})$$

where the $\mathcal{S}_i^{\mu_1\mu_2}$ denote tensor integrals. We can reduce the tensor integrals $\mathcal{S}_i^{\mu_1\mu_2}$ to scalar integrals S_k :

$$\mathcal{S}_i^{\mu_1\mu_2} = \sum_j T_j^{\mu_1\mu_2}(p_1, p_2, p_3, p_4) S_j. \quad (\text{B.8})$$

To achieve the above decomposition, we use a particular flavour of Passarino–Veltman tensor reduction [28]. The reduction of the tensor integrals is discussed here by writing only the integrand numerators $N^{\mu_1\mu_2}(k)$, keeping in mind that the identities exclusively hold at the integral level.

As a first step we strip off the external Lorentz structures factorising the loop momentum $N^{\mu_1\mu_2}(k)$ and write

$$N^{\mu_1\mu_2}(k) = c_0^{\mu_1\mu_2} + c_1^{\mu_1\mu_2;\alpha_1} k_{\alpha_1} + c_2^{\mu_1\mu_2;\alpha_1\alpha_2} k_{\alpha_1} k_{\alpha_2} + c_3^{\mu_1\mu_2;\alpha_1\alpha_2\alpha_3} k_{\alpha_1} k_{\alpha_2} k_{\alpha_3} + \dots, \quad (\text{B.9})$$

where the tensor coefficients c_i only involve γ -matrices, external momenta p_i and the metric tensor g . The tensor reduction is performed with the fully symmetric tensor numerators $\tilde{N}^{(\alpha_1\alpha_2\dots\alpha_n)}(k) = k^{\alpha_1} k^{\alpha_2} \dots k^{\alpha_n}$. Performing the loop integration of the tensor integral

$$\mathcal{S}_i^{(\alpha_1\alpha_2\dots\alpha_n)} = \int \frac{\tilde{N}^{(\alpha_1\alpha_2\dots\alpha_n)}(k)}{D_1 \dots D_{m_i}} d^D k = \sum_j t_j^{(\alpha_1\alpha_2\dots\alpha_n)}(g, p_1, p_2, p_3, p_4) c_j, \quad (\text{B.10})$$

will result in Lorentz tensors $t_j^{(\alpha_1\alpha_2\dots\alpha_n)}$ which are also completely symmetric in the internal Lorentz indices α_i . The symmetric tensor $t^{(\alpha_1\dots\alpha_n)}$ is given by

$$t^{(\alpha_1\dots\alpha_n)} = \frac{1}{n!} \sum_{\sigma \in \Sigma_n} t^{\alpha_{\sigma(1)}\dots\alpha_{\sigma(n)}}, \quad (\text{B.11})$$

where Σ_n is the symmetric group of order n , e.g.

$$t_{p_1, p_2}^{(\alpha_1\alpha_2)} = p_1^{\alpha_1} p_2^{\alpha_2} = \frac{1}{2} (p_1^{\alpha_1} p_2^{\alpha_2} + p_1^{\alpha_2} p_2^{\alpha_1}). \quad (\text{B.12})$$

Reduction with respect to a fully symmetric tensor basis reduces the number of tensor structures to be considered in the Ansatz significantly, while still remaining completely algorithmic.

A further simplification arises from the fact that the only underlying scalar topology depending on the full external kinematics p_1, p_2, p_3, p_4 is the pentagon displayed in Fig. 1a. Every other diagram will yield scalar integrals with reducible external kinematics yielding results depending on a reduced set of Mandelstam variables only. In general we group all

diagrams into families characterized by their minimal set of external momenta and perform the tensor reduction for the tensor numerators $\tilde{N}^{(\alpha_1\alpha_2\ldots\alpha_n)}(k)$ in each family separately with respect to the reduced external kinematics. This approach keeps the intermediate expressions obtained from tensor- and integration-by-parts (IBP) reduction very compact. The biggest matrix we have to invert is a 24×24 matrix for the rank 3 Lorentz tensor integrals of the pentagon diagram. To perform the analytic matrix inversion we employ the computer algebra system FERMAT [29], which takes below a minute on one core of a modern computer. In order to obtain the form factor in terms of scalar integrals we then insert the solutions back into (B.9).

With the tensor decomposition described, we are able to express the form factors for the QCD background and the vector-vector part of the weak contributions in terms of the following 20 tensor structures:

$$\begin{aligned}
T_1^{\mu_1\mu_2} &= \not{p}_1 \gamma^{\mu_1} \gamma^{\mu_2}, & T_2^{\mu_1\mu_2} &= \not{p}_2 \gamma^{\mu_1} \gamma^{\mu_2}, & T_3^{\mu_1\mu_2} &= g^{\mu_1\mu_2} \not{p}_1, & T_4^{\mu_1\mu_2} &= g^{\mu_1\mu_2} \not{p}_2, \\
T_5^{\mu_1\mu_2} &= \gamma^{\mu_1} p_3^{\mu_2}, & T_6^{\mu_1\mu_2} &= \gamma^{\mu_1} p_4^{\mu_2}, & T_7^{\mu_1\mu_2} &= \not{p}_1 \not{p}_2 \gamma^{\mu_1} p_3^{\mu_2}, & T_8^{\mu_1\mu_2} &= \not{p}_1 \not{p}_2 \gamma^{\mu_1} p_4^{\mu_2}, \\
T_9^{\mu_1\mu_2} &= \gamma^{\mu_2} p_3^{\mu_1}, & T_{10}^{\mu_1\mu_2} &= \not{p}_1 \not{p}_2 \gamma^{\mu_2} p_3^{\mu_1}, & T_{11}^{\mu_1\mu_2} &= \gamma^{\mu_2} p_4^{\mu_1}, & T_{12}^{\mu_1\mu_2} &= \not{p}_1 \not{p}_2 \gamma^{\mu_2} p_4^{\mu_1}, \\
T_{13}^{\mu_1\mu_2} &= \not{p}_1 p_3^{\mu_1} p_3^{\mu_2}, & T_{14}^{\mu_1\mu_2} &= \not{p}_2 p_3^{\mu_1} p_3^{\mu_2}, & T_{15}^{\mu_1\mu_2} &= \not{p}_1 p_3^{\mu_1} p_4^{\mu_2}, & T_{16}^{\mu_1\mu_2} &= \not{p}_2 p_3^{\mu_1} p_4^{\mu_2}, \\
T_{17}^{\mu_1\mu_2} &= \not{p}_1 p_3^{\mu_2} p_4^{\mu_1}, & T_{18}^{\mu_1\mu_2} &= \not{p}_2 p_3^{\mu_2} p_4^{\mu_1}, & T_{19}^{\mu_1\mu_2} &= \not{p}_1 p_4^{\mu_1} p_4^{\mu_2}, & T_{20}^{\mu_1\mu_2} &= \not{p}_2 p_4^{\mu_1} p_4^{\mu_2}.
\end{aligned} \tag{B.13}$$

B.2 Evaluation of scalar integrals

The IBP reduction of the remaining scalar integrals is performed using the program KIRA [30, 31]. We decompose the scalar pentagon integrals appearing as master integrals following ref. [32]. This decomposition relates the pentagon in $4 - 2\epsilon$ dimensions to a linear combination of all boxes obtainable by pinching one of the propagators, and the pentagon in $6 - 2\epsilon$ dimensions multiplied by a prefactor of order ϵ . Since the pentagon in six dimensions is finite, the additional term involving the six-dimensional pentagon is of order $\mathcal{O}(\epsilon)$ and can be omitted for the computation at hand.

We find that all form factors are finite diagram-by-diagram, but order $\mathcal{O}(\epsilon)$ coefficients of

the bubbles appear explicitly in the final amplitude.⁸ The relevant coefficients are given by

$$\begin{aligned} b_0(s; m^2, 0) &= h(\epsilon) \int \frac{1}{(k^2 - m^2)(k - p)^2} d^D k \\ &= \left(\frac{\mu^2}{m^2} \right)^\epsilon \left[\frac{1}{\epsilon} + 2 - \frac{(x-1) \ln(1-x)}{x} \right. \\ &\quad \left. + \left(4 + \frac{\pi^2}{6} + \frac{(1-x)}{2x} \left(2 \text{Li}_2 \left(-\frac{x}{1-x} \right) - \ln^2(1-x) + 4 \ln(1-x) \right) \right) \epsilon + \mathcal{O}(\epsilon^2) \right], \end{aligned} \quad (\text{B.14})$$

$$b_0(s; 0, 0) = h(\epsilon) \int \frac{1}{k^2(k-p)^2} d^D k = \left(-\frac{s}{\mu^2} \right)^{-\epsilon} \left[\frac{1}{\epsilon} + 2 + 4\epsilon + \mathcal{O}(\epsilon^2) \right], \quad (\text{B.15})$$

$$a_0(m) = h(\epsilon) \int \frac{1}{k^2 - m^2} d^D k = m^2 \left(\frac{\mu^2}{m^2} \right)^\epsilon \left[\frac{1}{\epsilon} + 1 + \left(1 + \frac{\pi^2}{6} \right) \epsilon + \mathcal{O}(\epsilon^2) \right], \quad (\text{B.16})$$

where $x = s/m^2$. The normalization

$$h(\epsilon) \equiv \frac{\mu^{2\epsilon}}{i\pi^{2-\epsilon}} \frac{\Gamma(1-2\epsilon)}{\Gamma(1-\epsilon)^2 \Gamma(\epsilon+1)}, \quad (\text{B.17})$$

is chosen to match the convention of ONELOOP [21], which is also used to evaluate the remaining non-trivial scalar master integrals.

In the evaluation of the expressions above, some care is needed in order to evaluate multi-valued functions on their physical Riemann sheet. The convention for numerical implementations of such functions is that the value assigned on the cut is the one coming around the finite endpoint of the cut in a counter-clockwise direction [33]. The Feynman prescription, however, dictates to replace s with $s + i\eta$ and take the limit $\eta \downarrow 0$, which gives

$$\lim_{\eta \downarrow 0} \ln \left(1 - \frac{s + i\eta}{m^2} \right) = \begin{cases} \ln(1-x) & s < m^2, \\ \ln(1-x) - 2i\pi & s > m^2, \end{cases} \quad (\text{B.18})$$

if the right-hand side respects the convention. The same holds for $s > 0$ in the expansion of the massless bubble. It is easy to see that for the dilogarithm in (B.14), instead, the physical sheet coincides with the conventional one for all $x \neq 1$.

B.3 Relations between the axial and vector parts of the amplitude

In the previous section we discussed the computation of the vector part $A_{gg \rightarrow d\bar{d}H}^{(0,2),VV}$. In what follows, we restrict the discussion to a single quark family with a diagonal CKM matrix, $g_V = g_V^*$ and $g_A = g_A^*$. The generalisation to all families of light quarks is straightforward and purely combinatorial. Since there are no closed fermion loops, we do not have to worry about ambiguous traces of γ^5 in $4 - 2\epsilon$ dimensions and we may take the D -dimensional γ^5 to be anticommuting.⁹

⁸This is particular to our approach and originates from the IBP reduction of the scalar integrals.

⁹Our choice corresponds to the NDR treatment of γ^5 (see e.g. [34]). Note however, that the amplitude is finite diagram by diagram and traces over γ^5 enter only in the interference of the AV-part with e.g. the QCD background. Since for the interference there is no explicit ϵ -dependence anymore, the traces can be treated as four-dimensional objects, without the need of imposing additional constraints.

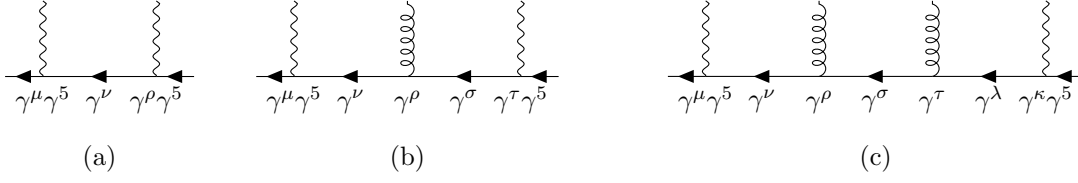


Figure 5: The relevant γ matrix structures for $A_{gg \rightarrow d\bar{d}H}^{(0,2),AA}$. Fig. 5a corresponds to triangle diagrams, Fig. 5b corresponds to box diagrams and Fig. 5c corresponds to pentagon diagrams.

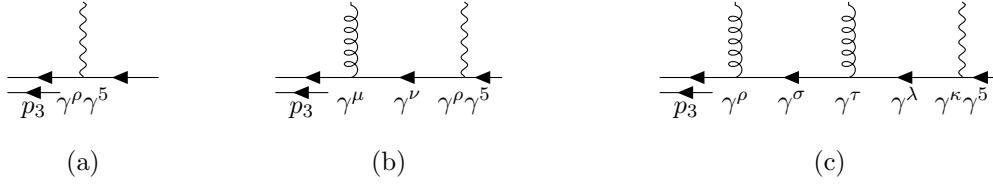


Figure 6: The relevant γ matrix structures for $A_{gg \rightarrow d\bar{d}H}^{(0,2),AV}$.

Within the purely axial amplitude $A_{gg \rightarrow d\bar{d}H}^{(0,2),AA}$ both weak couplings are $\propto g_A \gamma^\mu \gamma^5$. The γ chains that appear in the amplitude are shown in Fig. 5. One always needs to do an even number of anticommutations to arrive at $\gamma^5 \gamma^5 = \mathbb{1}$ from which immediately follows that

$$A_{gg \rightarrow d\bar{d}H}^{(0,2),AA} = \frac{|g_A|^2}{|g_V|^2} A_{gg \rightarrow d\bar{d}H}^{(0,2),VV}. \quad (\text{B.19})$$

The axial-vector piece $A_{gg \rightarrow d\bar{d}H}^{(0,2),AV}$ features the γ chains shown in Fig. 6. These chains represent the cases where only the vertex closest to the outgoing d quark (of momentum p_3) contributes with an axial coupling.¹⁰ It is easy to see that an uneven number of anticommutations is needed to bring γ^5 to the beginning of every spinor chain appearing in the process. The form factor for the AV part of the amplitude is therefore given by

$$\mathcal{F}_{AV}^{\mu\nu} = -2 \frac{g_A}{g_V} \gamma^5 \mathcal{F}_{VV}^{\mu\nu}. \quad (\text{B.20})$$

We thus conclude that the complete weak amplitude can be determined from its purely vector piece.

B.4 Ancillary files

The notation employed for the ancillary files is the following: We write every form factor in the ancillary files as the scalar product

$$\mathcal{F}_{s_1 s_2, l m}^{\mu\nu, ab} = (T_{s_1 s_2, l m}^{\mu\nu, ab})_i S_i, \quad (\text{B.21})$$

¹⁰The case where only the vertex “furthest” to the outgoing d quark contributes with the axial coupling is completely analogous.

where the vector T spans the direct product of colour and Lorentz spaces. The pairs of indices a, b and l, m are associated with the adjoint and fundamental representations of $SU(3)$ respectively; μ, ν are the Lorentz indices and s_1, s_2 are the spinor ones.

The interference between two amplitudes A and \tilde{A} in this notation then reads

$$\mathcal{M} = 2 \frac{1}{4} \frac{1}{(N_c^2 - 1)^2} \text{Re}(\tilde{s}_i^* B_{ij} s_j), \quad (\text{B.22})$$

where B is the *structure matrix* obtained summing over all colours, spins and polarisations:

$$B_{ij} = \sum \varepsilon_\mu(p_1) \varepsilon_\nu(p_2) \varepsilon_{\mu'}^*(p_1) \varepsilon_{\nu'}^*(p_2) u^{s'_1}(p_3) \bar{v}^{s'_2}(p_4) \bar{u}^{s_1}(p_3) v^{s_2}(p_4) \times (\tilde{T}_{s'_1 s'_2}^{\mu' \nu'})_i (T_{s_1 s_2}^{\mu \nu})_j. \quad (\text{B.23})$$

The ancillary files contain the vector $T_{s_1 s_2, lm}^{\mu \nu, ab}$ and the vector S for the QCD background, the VV and the AV part of the weak amplitude. We furthermore provide the structure matrices B for $A_{gg \rightarrow d\bar{d}H}^{(0,2), VV, (AA)} \mathcal{A}_{gg \rightarrow d\bar{d}H}^{*(2,0)}$ and $A_{gg \rightarrow d\bar{d}H}^{(0,2), AV, (VA)} \mathcal{A}_{gg \rightarrow d\bar{d}H}^{*(2,0)}$, which are sufficient to reproduce analytically the one-loop mixed QCD-weak matrix element for light quarks (excluding Higgsstrahlung contributions).

Appendix C Validation material

In order to facilitate the reproduction of our results, we provide below the numerical result for the matrix element $\mathcal{M}_{gg \rightarrow H d \bar{d}}^{(\alpha_s^3 \alpha^2)}$ and $\mathcal{M}_{gg \rightarrow H b \bar{b}}^{(\alpha_s^3 \alpha^2)}$ summed (averaged) over final (initial) state helicity and colour configurations for the following two kinematic points and $\alpha_s = 0.118$ (other SM parameters set to the values indicated in Table 2, unless otherwise stated).

The matrix elements computed are free of any explicit IR or UV divergence, so that the specific ϵ -dependent normalisation factor considered in MADLOOP's conventions is irrelevant in this case. For the two kinematic points shown in Table 7, we find:

[GeV]	E	p_x	p_y	p_z
$p_{g_1} =$	(500	, 0	, 0	, 500)
$p_{g_2} =$	(500	, 0	, 0	, -500)
$p_{h_3} =$	(467.7884686370085	, 166.5707878773001	, 373.1956790038965	, -190.2109596961058)
$p_{d_4} =$	(357.8737762854649	, -18.01807463012543	, -341.7897831227270	, 104.5405801225597)
$p_{\bar{d}_5} =$	(174.3377550775266	, -148.5527132471747	, -31.40589588116942	, 85.67037957354616)

(a) First kinematic configuration

[GeV]	E	p_x	p_y	p_z
$p_{g_1} =$	(500	, 0	, 0	, 500)
$p_{g_2} =$	(500	, 0	, 0	, -500)
$p_{h_3} =$	(503.1176012750793	, 183.7772678439759	, 314.6404088273092	, -323.6196064356687)
$p_{d_4} =$	(101.0581181325984	, -69.50635454208810	, -42.77041343901509	, 59.60118835247730)
$p_{\bar{d}_5} =$	(395.8242805923223	, -114.2709133018878	, -271.8699953882941	, 264.0184180831914)

(b) Second kinematic configuration

Figure 7: The two kinematic configurations used for the evaluation of the $\mathcal{O}(\alpha_s^3 \alpha^2)$ contribution to the process $gg \rightarrow H d \bar{d}$ presented in Table 4.

The first two matrix element evaluations given in Table 4 are exactly those used for obtaining the results of Table 3. The next six correspond to simplified setups that are only meant to ease comparisons against independent computations. More specifically, the matrix element denoted $\mathcal{M}_{gg \rightarrow H d \bar{d}}^{(\alpha_s^3 \alpha^2, \Gamma_{t,W^\pm,Z=0,W^\pm@[1a,1b,1c],VV)}$ corresponds to the case where:

- all widths are set to zero (then using on-shell renormalisation conditions)
- only the diagrams from the classes 1a, 1b and 1c with a W^\pm in the loop are kept
- only the vector part of the two W^\pm interactions is considered.

The definition of the last five matrix elements of the table is fully analogous, with 'AV+VA' indicating that the amplitude includes exactly one vector-like and one axial coupling of the electroweak boson to the quarks.

For each matrix element we checked numerical evaluations of the analytic result for 100 phase-space points and compare them against MADLOOP evaluations. We found perfect agreement at the level of the 10th digit on average.

[GeV ⁻²]	$\phi = \phi_{7a}$	$\phi = \phi_{7b}$
$\mathcal{M}_{gg \rightarrow H d \bar{d}}^{(\alpha_s^3 \alpha^2)}$	1.473268137642022e-11	-3.202714028092470e-09
$\mathcal{M}_{gg \rightarrow H b \bar{b}}^{(\alpha_s^3 \alpha^2)}$	-2.120437436454854e-09	-5.094650485339200e-09
$\mathcal{M}_{gg \rightarrow H d \bar{d}}^{(\alpha_s^3 \alpha^2, \Gamma_{t,W^\pm}=0, W^\pm @ [1a, 1b, 1c], VV)}$	1.046690169966104e-11	1.051226540819620e-10
Evaluation of analytic result	1.046690169966233e-11	1.051226540819659e-10
$\mathcal{M}_{gg \rightarrow H d \bar{d}}^{(\alpha_s^3 \alpha^2, \Gamma_{t,W^\pm}=0, W^\pm @ [1a, 1b, 1c], AV+VA)}$	-4.013450438936635e-11	-4.984414054112152e-10
Evaluation of analytic result	-4.013450438936742e-11	-4.984414054111984e-10
$\mathcal{M}_{gg \rightarrow H d \bar{d}}^{(\alpha_s^3 \alpha^2, \Gamma_{t,W^\pm}=0, W^\pm @ [1a, 1b, 1c], AA)}$	1.046690169966104e-11	1.051226540819620e-10
Evaluation of analytic result	1.046690169966233e-11	1.051226540819659e-10
$\mathcal{M}_{gg \rightarrow H d \bar{d}}^{(\alpha_s^3 \alpha^2, \Gamma_{t,Z}=0, Z @ [1a, 1b, 1c], VV)}$	2.656838076288246e-12	3.508375650188969e-11
Evaluation of analytic result	2.656838076288616e-12	3.508375650189406e-11
$\mathcal{M}_{gg \rightarrow H d \bar{d}}^{(\alpha_s^3 \alpha^2, \Gamma_{t,Z}=0, Z @ [1a, 1b, 1c], AV+VA)}$	-1.998115098837096e-11	-2.730298029116885e-10
Evaluation of analytic result	-1.998115098837179e-11	-2.730298029116787e-10
$\mathcal{M}_{gg \rightarrow H d \bar{d}}^{(\alpha_s^3 \alpha^2, \Gamma_{t,Z}=0, Z @ [1a, 1b, 1c], AA)}$	5.365688093206777e-12	7.085433478511003e-11
Evaluation of analytic result	5.365688093207525e-12	7.085433478511895e-11

Table 4: Benchmark evaluations of various matrix elements comparing numerical results from MADLOOP against an independent analytical derivation of the amplitude, presented in appendix B (see text for details).

The above matrix elements can readily be generated by MADLOOP (from within MG5AMC v2.6+) using commands similar¹¹ to the following which generates the matrix element $\mathcal{M}_{gg \rightarrow H d \bar{d}}^{(\alpha_s^3 \alpha^2)}$:

```

MG5_aMC> set complex_mass_scheme True
MG5_aMC> import loop_qcd_qed_sm
MG5_aMC> generate g g > h d d~ [virt=QCD QED] QED^2==4 QCD^2==6
MG5_aMC> output my_gg_hddx
MG5_aMC> launch -f

```

Note that in order to select only the diagrams of the classes 1a, 1b and 1c, the following

¹¹See <https://cp3.irmp.ucl.ac.be/projects/madgraph/wiki/MadLoopStandaloneLibrary> for instructions on how to generate the corresponding standalone library for linking against your own code.

--loop_filter option ¹² can be passed to the following generate command, yielding the matrix element $\mathcal{M}_{gg \rightarrow H d \bar{d}}^{(\alpha_s^3 \alpha^2, \Gamma_{t, W^\pm, Z=0, Z@[1a, 1b, 1c], VV+AV+VA+AA)}$:

```
MG5_aMC> generate g g > h d d~ / w+ w- a [virt=QCD QED] QED^2==4 QCD^2==6
--loop_filter=not(23\\ in\\ struct_pdgs\\ or\\ 250\\ in\\ struct_pdgs)
```

References

- [1] C. Anastasiou, C. Duhr, F. Dulat, F. Herzog, and B. Mistlberger, *Higgs Boson Gluon-Fusion Production in QCD at Three Loops*, *Phys. Rev. Lett.* **114** (2015) 212001, [[1503.06056](#)].
- [2] B. Mistlberger, *Higgs boson production at hadron colliders at N^3LO in QCD*, *JHEP* **05** (2018) 028, [[1802.00833](#)].
- [3] C. Anastasiou, C. Duhr, F. Dulat, E. Furlan, T. Gehrmann, F. Herzog, A. Lazopoulos, and B. Mistlberger, *High precision determination of the gluon fusion Higgs boson cross-section at the LHC*, *JHEP* **05** (2016) 058, [[1602.00695](#)].
- [4] U. Aglietti, R. Bonciani, G. Degrossi, and A. Vicini, *Two loop light fermion contribution to Higgs production and decays*, *Phys. Lett.* **B595** (2004) 432–441, [[hep-ph/0404071](#)].
- [5] S. Actis, G. Passarino, C. Sturm, and S. Uccirati, *NLO Electroweak Corrections to Higgs Boson Production at Hadron Colliders*, *Phys. Lett.* **B670** (2008) 12–17, [[0809.1301](#)].
- [6] S. Actis, G. Passarino, C. Sturm, and S. Uccirati, *NNLO Computational Techniques: The Cases $H \rightarrow \gamma\gamma$ and $H \rightarrow gg$* , *Nucl. Phys.* **B811** (2009) 182–273, [[0809.3667](#)].
- [7] C. Anastasiou, R. Boughezal, and F. Petriello, *Mixed QCD-electroweak corrections to Higgs boson production in gluon fusion*, *JHEP* **04** (2009) 003, [[0811.3458](#)].
- [8] M. Bonetti, K. Melnikov, and L. Tancredi, *Three-loop mixed QCD-electroweak corrections to Higgs boson gluon fusion*, *Phys. Rev.* **D97** (2018), no. 3 034004, [[1711.11113](#)].
- [9] M. Bonetti, K. Melnikov, and L. Tancredi, *Higher order corrections to mixed QCD-EW contributions to Higgs boson production in gluon fusion*, *Phys. Rev.* **D97** (2018), no. 5 056017, [[1801.10403](#)]. [Erratum: *Phys. Rev.* **D97**, no. 9, 099906 (2018)].

¹² Also note that the rather long loop filters indicated on the command line can alternatively be specified directly in the user-function `user_filter()` of the MG5AMC PYTHON module `loop_diagram_generation.py`.

- [10] C. Anastasiou, V. Del Duca, E. Furlan, B. Mistlberger, F. Moriello, A. Schweitzer, and C. Specchia, *Mixed QCD-electroweak corrections to Higgs production via gluon fusion in the small mass approximation*, [1811.11211](#).
- [11] A. Denner, *Techniques for calculation of electroweak radiative corrections at the one loop level and results for W physics at LEP-200*, *Fortsch. Phys.* **41** (1993) 307–420, [[0709.1075](#)].
- [12] R. Frederix, S. Frixione, V. Hirschi, D. Pagani, H. S. Shao, and M. Zaro, *The automation of next-to-leading order electroweak calculations*, *JHEP* **07** (2018) 185, [[1804.10017](#)].
- [13] G. Degrossi and F. Maltoni, *Two-loop electroweak corrections to Higgs production at hadron colliders*, *Phys. Lett.* **B600** (2004) 255–260, [[hep-ph/0407249](#)].
- [14] G. Somogyi, *Subtraction with hadronic initial states at NLO: An NNLO-compatible scheme*, *JHEP* **05** (2009) 016, [[0903.1218](#)].
- [15] R. V. Harlander, J. Vollinga, and M. M. Weber, *Gluon-Induced Weak Boson Fusion*, *Phys. Rev.* **D77** (2008) 053010, [[0801.3355](#)].
- [16] V. Hirschi, R. Frederix, S. Frixione, M. V. Garzelli, F. Maltoni, and R. Pittau, *Automation of one-loop QCD corrections*, *JHEP* **05** (2011) 044, [[1103.0621](#)].
- [17] J. Alwall, R. Frederix, S. Frixione, V. Hirschi, F. Maltoni, O. Mattelaer, H. S. Shao, T. Stelzer, P. Torrielli, and M. Zaro, *The automated computation of tree-level and next-to-leading order differential cross sections, and their matching to parton shower simulations*, *JHEP* **07** (2014) 079, [[1405.0301](#)].
- [18] V. Hirschi and O. Mattelaer, *Automated event generation for loop-induced processes*, *JHEP* **10** (2015) 146, [[1507.00020](#)].
- [19] T. Peraro, *Ninja: Automated Integrand Reduction via Laurent Expansion for One-Loop Amplitudes*, *Comput. Phys. Commun.* **185** (2014) 2771–2797, [[1403.1229](#)].
- [20] V. Hirschi and T. Peraro, *Tensor integrand reduction via Laurent expansion*, *JHEP* **06** (2016) 060, [[1604.01363](#)].
- [21] A. van Hameren, *OneLOop: For the evaluation of one-loop scalar functions*, *Comput. Phys. Commun.* **182** (2011) 2427–2438, [[1007.4716](#)].
- [22] A. Denner, S. Dittmaier, and L. Hofer, *Collier: a fortran-based Complex One-Loop Library in Extended Regularizations*, *Comput. Phys. Commun.* **212** (2017) 220–238, [[1604.06792](#)].

- [23] W.-Y. Keung and F. J. Petriello, *Electroweak and finite quark-mass effects on the Higgs boson transverse momentum distribution*, *Phys. Rev.* **D80** (2009) 013007, [[0905.2775](#)].
- [24] X. Chen, J. Cruz-Martinez, T. Gehrmann, E. W. N. Glover, and M. Jaquier, *NNLO QCD corrections to Higgs boson production at large transverse momentum*, *JHEP* **10** (2016) 066, [[1607.08817](#)].
- [25] S. Catani and M. H. Seymour, *A General algorithm for calculating jet cross-sections in NLO QCD*, *Nucl. Phys.* **B485** (1997) 291–419, [[hep-ph/9605323](#)]. [Erratum: Nucl. Phys.B510,503(1998)].
- [26] P. Nogueira, *Automatic Feynman graph generation*, *J. Comput. Phys.* **105** (1993) 279–289.
- [27] J. A. M. Vermaseren, *New features of FORM*, [math-ph/0010025](#).
- [28] G. Passarino and M. J. G. Veltman, *One Loop Corrections for $e^+ e^-$ Annihilation Into $\mu^+ \mu^-$ in the Weinberg Model*, *Nucl. Phys.* **B160** (1979) 151–207.
- [29] R. H. Lewis, “Computer Algebra System Fermat.” <https://home.bway.net/lewis/>.
- [30] P. Maierhöfer, J. Usovitsch, and P. Uwer, *Kira—A Feynman integral reduction program*, *Comput. Phys. Commun.* **230** (2018) 99–112, [[1705.05610](#)].
- [31] P. Maierhöfer and J. Usovitsch, *Kira 1.2 Release Notes*, [1812.01491](#).
- [32] Z. Bern, L. J. Dixon, and D. A. Kosower, *Dimensionally regulated one loop integrals*, *Phys. Lett.* **B302** (1993) 299–308, [[hep-ph/9212308](#)]. [Erratum: Phys. Lett.B318,649(1993)].
- [33] B. S. Institution, *The C standard: incorporating Technical Corrigendum 1 : BS ISO/IEC 9899/1999*. John Wiley, 2003.
- [34] F. Jegerlehner, *Facts of life with $\gamma(5)$* , *Eur. Phys. J.* **C18** (2001) 673–679, [[hep-th/0005255](#)].